TFLN MZMs and Next-Gen DACs: Enabling Beyond 400 Gbps IMDD O-Band and C-Band Transmission

Essam Berikaa[ID], *Graduate Student Member, IEEE*, Md Samiul Alam[ID], *Graduate Student Member, IEEE*, Weijia Li[ID], *Graduate Student Member, IEEE*, Santiago Bernal, Benjamin Krueger, Fabio Pittalà, and David V. Plant, *Fellow, IEEE*

Abstract— **As internet traffic demand continues to increase, high-speed electro-optic modulators and high-bandwidth RF components are needed to stretch intensity modulation direct detection (IMDD) systems to their limits. In this study, we experimentally demonstrate the transmission performance using the next generation of digital-to-analog converters (DAC) and high-bandwidth thin-film lithium niobate (TFLN) modulators. In the C-band, we transmit 172 Gbaud PAM6 and 180 Gbaud PAM8 over 120 m of SSMF under the 6.7% overhead hard-decision forward error correction (HD-FEC) and the 20% overhead soft-decision (SD)-FEC thresholds, which respectively correspond to net 400 and 450 Gbps. We also demonstrate the first transmission of net 400 Gbps over 10 km in the O-band (1310 nm) using 172 Gbaud probabilistically shaped (PS)-PAM8 under the 20% SD-FEC BER threshold. Our results indicate that the TFLN platform has the potential to support even higher data rates with the development of high-bandwidth RF components.**

Index Terms— **Datacenter interconnects, thin-film lithium niobate, pulse amplitude modulation, digital-to-analog converters.**

I. INTRODUCTION

WITH the rise of bandwidth-hungry applications like Metaverse, cloud-based services, artificial intelligence applications, and streaming platforms, the demand for data traffic is growing rapidly. This has led to a strain on the capacity of short-reach datacenter interconnects (DCI) employing cost-effective IMDD solutions, which struggle to keep up with the traffic demand. The 200 G/λ specifications have been defined [1]; however, 400 G/λ is still an open question as it requires operating at higher symbol rates, which challenges the bandwidth of the electro-optic modulators and the RF componentry.

The announcement of the development of 1.6 Tbps/λ commercial coherent transceivers is a significant milestone for
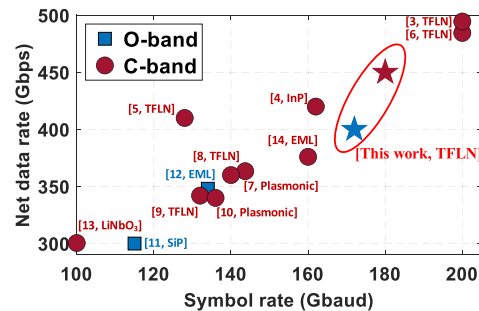
Fig. 1.   Summary of the high-speed IMDD demonstrations.

the optical telecommunication industry [2]. These transceivers support 200 Gbaud operation and are built using 3 nm CMOS technology. This announcement marks the beginning of a new era for digital signal processor (DSP) ASICs and highlights the direction the industry is taking towards higher symbol rates and bandwidth requirements (∼100 GHz).

To overcome bandwidth limitations and demonstrate 400 G/λ IMDD systems, researchers adopted different configurations. Recent high-speed IMDD reports are summarized in Fig. 1 [3], [4], [5], [6], [7], [8], [9], [10], [11], [12], [13], [14]. The majority of the reports are in the C-band. Here we report the both the C-band and O-band transmission performance, motivated by the higher achieved throughput with the C-band MZM, and to highlight the potential transmission performance in conventional C-band coherent tarnsmisison based on the C-band TFLN MZM structure. Using three interleaved DACs and TFLN C-band Mach–Zehnder modulator (MZM), the authors of [3] reported the transmission of 200 Gbaud PS-PAM16 (net 494.5 Gbps) over 120 m. Another work utilized an analog multiplexer (AMUX) to generate and transmit 162 Gbaud PS-PAM16 (net 420 Gbps) [4]. In our previous work, we showed that a single DAC channel could operate at 128 Gbaud PAM16 (net 410 Gbps) assuming 25% overhead SD-FEC [5]. However, the high signal-to-noise ratio (SNR) requirement of PAM16 poses a challenge to its practical adoption and deployment. The majority of the reports are in the C-band. Here we report both the C-band and O-band transmission performance, motivated by the higher achieved throughput with the C-band MZM, and to highlight the design tradeoffs as the two MZMs have different specifications. The C-band data provides valuable insights into the potential performance of conventional C-band coherent transmission based on C-band TFLN MZM structure. However, we do not

Fig. 2. The TFLN MZMs characteristics: (a) the electro-optic (EO) response, and (b) the RF Vπ.

Fig. 3. The C-band experimental setup and DSP routines.

TABLE I
SUMMARY OF NET BITRATE ACHIEVED

		C-band MZM		O-band MZM	
FEC	Overhead	Format	Net rate (Gbps)	Format	Net rate (Gbps)
KP4-FEC	5.4 %	164 Gbaud PAM4	310	136 Gbaud PAM4	258
HD-FEC	6.7 %	172 Gbaud PAM6	402	176 Gbaud PAM4	330
SD-FEC	20 %	180 Gbaud PAM8	450	172 Gbaud PS-PAM8	400
SD-FEC	25 %	192 Gbaud PAM8	460	170 Gbaud PAM8	408

consider TFLN-based C-band IMDD systems a viable solution for short-reach interconnects.

The objective of this study is to assess the effectiveness of employing the latest generation of DACs and RF drivers with the TFLN platform. Specifically, the study utilizes Keysight's M8199B arbitrary waveform generator (AWG) with both O-band and C-band TFLN MZMs. The AWG works at 256 GSa/s with an integrated interleaver and RF driver, which supports operating beyond 85 GHz with a sufficiently high driving swing for the TFLN MZMs. In this letter, we demonstrate the transmission of 180 Gbaud PAM8 with the C-band MZM and 172 Gbaud PS-PAM8 with the O-band MZM under the 20% overhead SD-FEC BER threshold, achieving net data rates of 450 and 400 Gbps, respectively.

II. TRANSMISSION EXPERIMENT

In this work, we employ C-band and O-band MZMs with different designs and specifications as shown in Fig. 2. The C-band MZM has 23 mm coplanar electrodes with nearly 50 Ω on-chip termination and is optically connected with vertical grating couplers. It has a fiber-to-fiber insertion loss (IL) of 12 dB at peak transmission (including grating couplers loss) and a DC optical extinction ratio (ER) of more than 26 dB. The O-band MZM has 18 mm electrodes with similar termination and is connected via edge couplers. Unfortunately, due to a layout and fabrication error, the O-band MZM has a fiber-to-fiber IL of 24 dB with a modest DC optical ER of 20 dB. However, this error does not affect the MZM's RF characteristics.

A critical factor in evaluating the performance of IMDD links is the achievable link power budget. The commercial-grade TFLN MZM exhibits an insertion loss of 4.5 dB, including the coupling loss. Additionally, intensity modulation introduces an extra 3 dB loss for linear modulation at the MZM quadrature point. For 2 km transmission in the O-band, the fiber loss is ~1 dB, including losses from connectors. A further 1.5 dB loss occurs during coupling into the receiver chip since the TFLN platform does not have photodiodes. To accommodate multiple IMDD channels, an additional 4 dB loss is considered due to the optical Mux/Demux. Consequently, the overall link power budget of TFLN-based IMDD link amounts to 14 dB, which can be supported by existing commercial products. However, it is important to note that this calculation does not account for the penalty resulting from dispersion or include any margin for implementation penalties.

The C-band MZM has previously been used in [5], and it has a 24 (66) GHz 3-(6-) dB bandwidth, while the O-band MZM has a 3-dB bandwidth of more than 70 GHz, as shown in Fig. 2(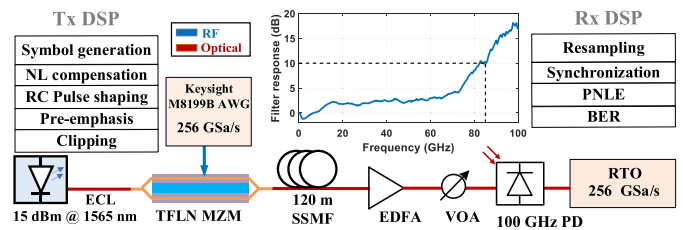a). The RF Vπ is measured at 20 GHz and extrapolated based on the MZM's frequency response, as illustrated in Fig. 2(b). The low-MHz Vπ of the C-band and O-band MZMs are respectively 1.25 V and 1.7 V, which increase to 3.3 V and 2.9 V at 90 GHz.

A. C-Band Transmission Performance

Fig. 3 depicts the experimental setup and DSP routine employed in the C-band transmission experiment, which follows the conventional IMDD architecture except for employing an optical amplifier to compensate for the extra IL from the modulator and the absence of a trans-impedance amplifier (TIA) [8]. We first generate 2^{19} random PAM symbols by Mersenne twister, and then we pre-distort the symbols based on a non-linear lookup table with a 3-symbols memory length [15]. Then the symbols are filtered with a raised cosine (RC) pulse-shaping filter. The pulse-shaped signal is upsampled to 256 GSa/s, filtered with the digital pre-emphasis filter shown in the inset of Fig. 3, and clipped to limit its peak-to-average power ratio (PAPR) before loading to the AWG. The digital pre-emphasis filter compensates for the frequency response of the AWG (DAC and internal driver) and 20 cm of 1 mm connectorized RF cable.

Optically, a 15 dBm external cavity laser (ECL) at 1565 nm is used, which corresponds to the peak transmission of the vertical grating couplers. The output of the MZM is transmitted over 120 m to minimize the impact of chromatic dispersion (2 ps/nm). Then the signal is amplified by an EDFA to 7 dBm. The variable optical attenuator (VOA) is added to sweep the received optical power (ROP) reaching the 100 GHz photodiode (PD). The output of the PD is digitized for processing by a 105 GHz real-time oscilloscope (RTO). The receiver DSP is carried out at 2 samples per second (sps) using a 2nd order polynomial nonlinear equalizer (PNLE) [16], before BER calculation.

The C-band transmission performance is summarized in Fig. 4 and Table I. Fig. 4(a) shows the BER versus the symbol rate for the different PAM formats at 7 dBm ROP. The PAM6 symbols are derived from the standard cross 32QAM
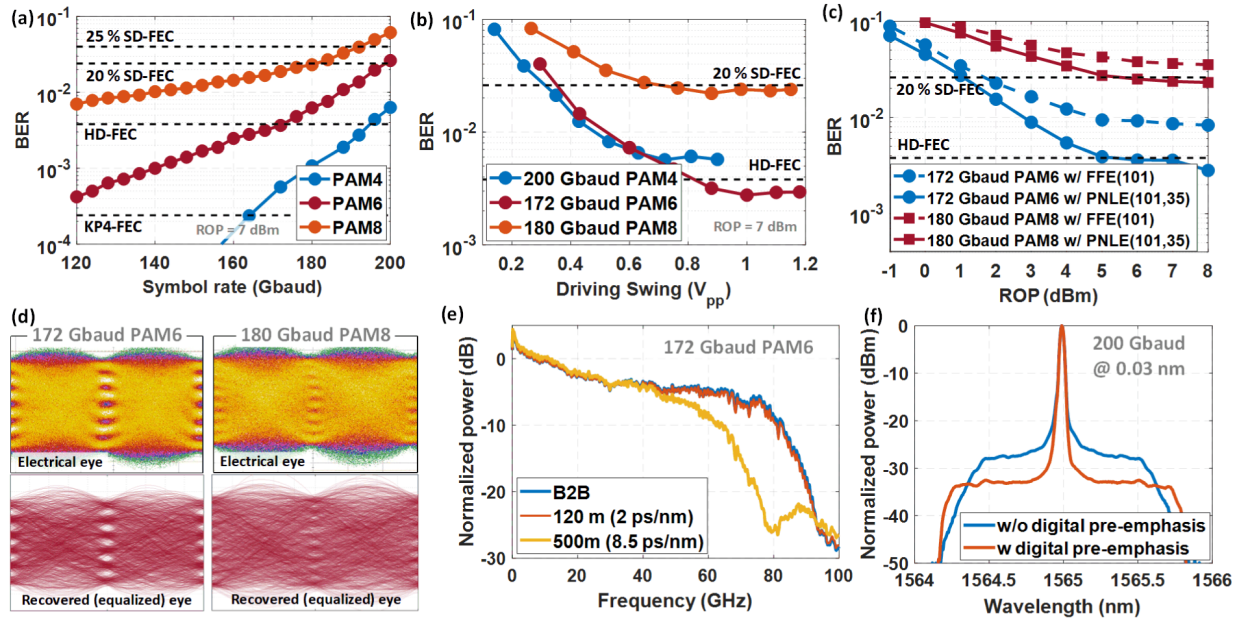
Fig. 4. The C-band transmission performance. (a) The BER versus the symbol rate. (b) The BER versus the driving swing after digital pre-emphasis. (c) The BER versus the ROP. (d) The eye diagrams of the AWG output and the corresponding equalized signals. (e) The received RF spectra of 172 Gbaud PAM6 at different dispersion levels. (f) The optical spectra after the MZM of 200 Gbaud PAM4 with and without digital pre-emphasis.

constellation with a pseudo-Gray bit mapping, which has a gray mapping penalty of 1.1667. We transmit 164 Gbaud PAM4 and 172 Gbaud PAM6 under the KP4-FEC and the 6.7% overhead HD-FEC thresholds, which corresponds to net 310 and 402 Gbps, respectively. To our knowledge, this is the first demonstration of a net data rate of 400 Gbps employing a standard PAM format at the 6.7% HD-FEC threshold, which has significant implications for power consumption and latency. Additionally, we demonstrate the transmission of 180 Gbaud PAM8 under the 2.4×10^{-2} 20% overhead SD-FEC BER threshold corresponding to a net data rate of 450 Gbps, which is the highest reported data rate using a commercial DAC under these FEC conditions.

Fig. 4(b) shows the BER versus the driving swing into the MZM. The AWG has an internal driver capable of providing up to 2.5 V_{pp} single-ended output; however, the digital pre-emphasis filter and the high PAPR reduce the actual output driving swing. The reported values are measured using the electrical head of a 100 GHz digital communication analyzer (DCA). Our measurements demonstrate that a driving swing of only 1 V_{pp} is sufficient for achieving the reported performance, which is attributed to the low V_π of the TFLN MZM. This relaxes the requirements on the driver swing, letting the designers focus more on improving the bandwidth.

Fig. 4 (c) shows the BER sensitivity to the ROP of 172 Gbaud PAM6 and 180 Gbaud PAM8 using a linear feed-forward equalizer, and a 2nd order PNLE to assess the linearity of the received signal. The BER reaches the error floor at ROP of 5 dB. Although PAM8 suffers more from non-linearity, the gain for PAM6 is higher because of PAM8's higher SNR requirement, and the lengths of the equalizer kernels are indicated in the figure. Fig. 4(d) shows the eye diagrams of the RF signal before the MZM and after processing at the receiver with PNLE. The RF signal eye diagrams reveal that the non-linearity in the signal stems from the non-linear
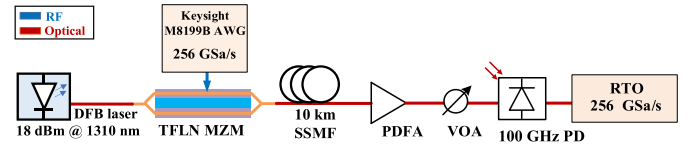
transfer function of the AWG internal driver, whereas the eye-opening decreases with the increases in signal level.

The impact of chromatic dispersion is illustrated in Fig. 4(e) by transmitting the signal over different fiber lengths. The power fading observed for 500 m (8.5 ps/nm) transmission at 80 GHz is due to chromatic dispersion, which imposes a fundamental limit on the reach of high symbol rate IMDD systems. Fig. 4(f) shows the optical spectra of 200 Gbaud PAM4 signals after the MZM with and without digital pre-emphasis. The difference in signal power between the two spectra arises from the reduction in driving swing after pre-emphasis. Nonetheless, the digital pre-emphasis is essential for transmitting high symbol rate signals beyond 150 Gbaud.

B. O-Band Transmission Performance

Fig. 5 shows the modified experimental setup for O-band operation. To operate in the O-band, we utilize an 18 dBm DFB laser at 1310 nm, which is near the zero dispersion wavelength and allows for transmission up to 10 km. Due to fabrication error, the MZM IL is fairly high at 24 dB, so we use a 2-stage PDFA with a noise figure of 6.5 dB to amplify the signal to 7 dBm. Moreover, the additional noise introduced by the PDFA and the lower ER of the O-band MZM result in inferior overall performance compared to the C-band MZM.

In Fig. 6, we present a summary of the O-band transmission performance, which is summarized by Table I. Fig. 6(a) shows

Fig. 5. Modified experimental setup for the O-band transmission experiment.
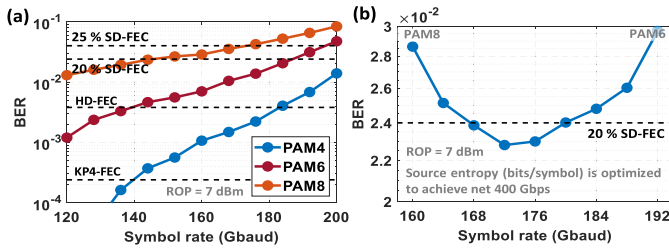
Fig. 6. The O-band transmission performance. (a) The BER versus the symbol rate. (b) The BER versus the symbol rate of PS-PAM8 with optimized entropies to achieve net 400 Gbps assuming 20% overhead.

the impact of symbol rate and PAM order on the BER. We transmit 170 Gbaud PAM8 signals under the 4×10^{-2} 25% overhead SD-FEC BER threshold, achieving a net rate of 408 Gbps. However, achieving a net rate of 400 Gbps under the 20% SD-FEC threshold with standard PAM modulation is not feasible. Therefore, we adopt the PS-PAM8 format and optimize the source entropy to achieve a net rate of 400 Gbps under the 20% SD-FEC threshold, as depicted in Fig. 6(b). The PS-PAM8 signals are generated using a constant composition distribution matcher (CCDM) with a Maxwell–Boltzmann distribution [17]. The PS format improves the performance by leveraging the trade-off between bandwidth limitations and SNR requirements, offering a finer spectral efficiency granularity. With PS-PAM8, we transmit 172 Gbaud at a source entropy of 2.79 bits/symbol under the 20% SD-FEC BER threshold, resulting in a net rate of 400 Gbps. This is the first demonstration of net 400 Gbps transmission in the O-band and over a distance of 10 km.

This work demonstrates the transmission of net 400 Gbps in the O-band over a distance of 10 km. However, it may be premature to consider $4\lambda \times 400$ G for 1.6 T solutions over a range of 2 to 10 km. Currently, 800 G IMDD solutions rely on CWDM with either $4\lambda \times 200$ G or $8\lambda \times 100$ G and are standardized for a reach of up to 2 km. 1.6 T can be achieved in different configurations, including $16\lambda \times 100$ G, $8\lambda \times 200$ G, and $4\lambda \times 400$ G. The 4λ approach is preferred due to its simpler architecture and lower device count, but it requires a high symbol rate that is not feasible at the edge channels of the CWDM grid. One solution is to modify the WDM grid to concatenate the 4λ in smaller bandwidth near the zero dispersion wavelength, but this is challenging due to channel non-linearities and four-wave mixing (FWM). Yet, transmitting four fibers over 10 km is not cost-effective. Therefore, efforts are exerted to optimize the WDM grid for such high symbol rate systems and possible ways to mitigate FWM. This is still a question that requires significant joint efforts from both academia and the industry to address.

III. CONCLUSION

This study examines the performance achievable by utilizing the next generation of RF componentry in combination with high-bandwidth TFLN MZMs. Our testbed employed Keysight's M8199B AWG with more than 85 GHz of operational bandwidth and a 100 GHz compliant receiver. We demonstrate the successful transmission of net 400 Gbps in the C-band over 120 m assuming the 6.7% overhead HD-FEC

using 172 Gbaud PAM6. This can be increased to net 450 Gbps with 180 Gbaud PAM8, assuming 20% SD-FEC. In the O-band (1310 nm) and over 10 km of SSMF, we achieve net 400 Gbps transmission through 172 PS-PAM8 and the 20% SD-FEC. Our results demonstrate the potential of the TFLN platform for next-generation DCIs, and reveal that the limiting factor in previous studies was the RF componentry bandwidth rather than the TFLN technology itself.

REFERENCES

[1] *800G Pluggable MSA*. Accessed: Mar. 25, 2023. [Online]. Available: https://www.800gmsa.com/

[2] S. McFeely. *Introducing WaveLogic 6: Another Industry First From Ciena*. Accessed: Mar. 25, 2023. [Online]. Available: https://www.ciena.com/

[3] D. Che and X. Chen, "Higher-order modulation vs faster-than-Nyquist PAM-4 for datacenter IM-DD optics: An AIR comparison under practical bandwidth limits," *J. Lightw. Technol.*, vol. 40, no. 10, pp. 3347–3357, May 15, 2022.

[4] H. Yamazaki et al., "Net-400-Gbps PS-PAM transmission using integrated AMUX-MZM," *Opt. Exp.*, vol. 27, no. 18, pp. 25544–25550, 2019.

[5] E. Berikaa, M. S. Alam, and D. V. Plant, "Net 400-Gbps/λ IMDD transmission using a single-DAC DSP-free transmitter and a thin-film lithium niobate MZM," *Opt. Lett.*, vol. 47, no. 23, pp. 6273–6276, 2022.

[6] X. Chen et al., "Single-wavelength and single-photodiode 700 Gb/s entropy-loaded PS-256-QAM and 200-GBaud PS-PAM-16 transmission over 10-km SMF," in *Proc. Eur. Conf. Opt. Commun. (ECOC)*, Dec. 2020, pp. 1–4.

[7] Q. Hu et al., "Ultrahigh-net-bitrate 363 Gbit/s PAM-8 and 279 Gbit/s polybinary optical transmission using plasmonic Mach–Zehnder modulator," *J. Lightw. Technol.*, vol. 40, no. 10, pp. 3338–3346, May 15, 2022.

[8] M. S. Alam, E. Berikaa, and D. V. Plant, "Net 350 Gbps/λ IMDD transmission enabled by high bandwidth thin-film lithium niobate MZM," *IEEE Photon. Technol. Lett.*, vol. 34, no. 19, pp. 1003–1006, Oct. 1, 2022.

[9] E. Berikaa, M. S. Alam, and D. V. Plant, "Beyond 300 Gbps short-reach links using TFLN MZMs with 500 mVpp and linear equalization," *IEEE Photon. Technol. Lett.*, vol. 35, no. 3, pp. 140–143, Feb. 1, 2023.

[10] M. Eppenberger et al., "Plasmonic racetrack modulator transmitting 220 Gbit/s OOK and 408 Gbit/s 8 PAM," in *Proc. Eur. Conf. Opt. Commun. (ECOC)*, Sep. 2021, pp. 1–4.

[11] M. S. Alam, X. Li, M. Jacques, E. Berikaa, P.-C. Koh, and D. V. Plant, "Net 300 Gbps/λ transmission over 2 km of SMF with a silicon photonic Mach–Zehnder modulator," *IEEE Photon. Technol. Lett.*, vol. 33, no. 24, pp. 1391–1394, Dec. 15, 2021.

[12] M. S. Bin Hossain et al., "402 Gb/s PAM-8 IM/DD O-band EML transmission," in *Proc. Eur. Conf. Opt. Commun. (ECOC)*, Sep. 2021, pp. 1–4.

[13] J. Zhang et al., "Nonlinearity-aware PS-PAM-16 transmission for C-band net-300-Gbit/s/λ short-reach optical interconnects with a single DAC," *Opt. Lett.*, vol. 47, no. 12, pp. 3035–3038, 2022.

[14] O. Ozolins et al., "Optical amplification-free 310/256 Gbaud OOK, 197/145 Gbaud PAM4, and 160/116 Gbaud PAM6 EML/DML-based data center links," in *Proc. Opt. Fiber Commun. Conf. (OFC)*, 2023, p. Th4B.2.

[15] T. Rahman, S. Calabro, N. Stojanovic, L. Zhang, J. Wei, and C. Xie, "LUT-assisted pre-compensation for 225 Gb/s/λ O-band transmission," in *Proc. 45th Eur. Conf. Opt. Commun. (ECOC)*, Sep. 2019, pp. 1–4.

[16] E. L. O. Batista and R. Seara, "On the performance of adaptive pruned Volterra filters," *Signal Process.*, vol. 93, no. 7, pp. 1909–1920, Jul. 2013.

[17] P. Schulte and G. Böcherer, "Constant composition distribution matching," *IEEE Trans. Inf. Theory*, vol. 62, no. 1, pp. 430–434, Jan. 2016.